A β”-Alumina/Inorganic Ionic Liquid Dual Electrolyte for Intermediate-temperature Sodium-sulfur Batteries

Di Wang, Jinkwang Hwang, Chi-yao Chen, Keigo Kubota, Kazuhiko Matsumoto, Rika Hagiwara*

Di Wang, Prof. J. Hwang, Prof. K. Matsumoto, Prof. R. Hagiwara
Graduate School of Energy Science, Kyoto University, Yoshida-honmachi, Sakyo-ku, Kyoto 606-8501, Japan
E-mail: k-matsumoto@energy.kyoto-u.ac.jp

Prof. J. Hwang, Prof. K. Matsumoto, Prof. R. Hagiwara
Unit of Elements Strategy Initiative for Catalysts & Batteries (ESICB), Kyoto University, Katsura, Kyoto 615-8510, Japan

Dr. C.-Y. Chen, Dr. K. Kubota, Prof. K. Matsumoto, Prof. R. Hagiwara AIST-Kyoto University Chemical Energy Materials Open Innovation Laboratory (ChEM-OIL), Sakyo–ku, Kyoto 606–8501, JAPAN

Keywords: sodium-sulfur battery, intermediate-temperature, electrolyte, ionic liquid, molten salt

Although sodium-sulfur (Na-S) batteries present the great prospects of high energy density, long cycleability, and sustainability, their deployment is heavily encumbered by safety, practicality and versatility issues engendered by their high operating temperatures above 300 °C. Lowering the operating temperatures significantly impedes the performance of Na-S batteries due to the formation of electrical insulating S/polysulfides, diminished Na ion conduction in the β”-alumina solid electrolyte, the Na metal dendrite growth at temperatures below its melting point, and the shuttle effect occurring in absence of the β”-alumina solid electrolyte. Herein, we propose a Na-S battery that integrates a dual electrolyte consisting of the β”-alumina solid electrolyte and a novel inorganic ionic liquid for intermediate-temperature operations of 150 °C. Investigations reveal the ionic liquid to have high ionic conductivity, wide electrochemical window of 5.1 V as well as excellent thermal and chemical stability, making it propitious for intermediate-temperature operations. The system demonstrates a high reversible capacity of 795 mAh $(g\text{-}S)^{-1}$ at 0.1 mA (electrode area: 0.785 cm^2). Moreover, an average capacity of 381 mAh $(g\text{-}S)^{-1}$ is achieved over 1000 cycles at 0.5 mA, unprecedented for intermediate-temperature Na-S batteries. These exceptional results validate the use of ionic liquids in dual electrolyte systems as a strategy to improve Na-S performance.

1. Introduction

Energy storage systems, most notably rechargeable batteries, play a pivotal role in the deployment of renewable energy applications, particularly in regulating power supply from variable and intermittent sources such as solar, tide, and wind.[1–3] Among the numerous rechargeable batteries developed for large-scale storage applications, sodium-sulfur (Na-S) batteries have garnered widespread attention for their high energy density, low cost, and abundance of raw materials. As a result, these batteries are uniquely suited for practical grid applications such as load balancing and emergency power supply.[4]

In ideal Na-S battery, energy is dispensed through reversible electrochemical reactions that entail the formation of polysulfides (Na_2S_x; it should be noted that x does not always mean such a solid single phase exists.[4]) at the positive electrode, achieving theoretical capacities ranging from 209 (x = 8) to 1672 (x = 1) mAh (g-S)$^{-1}$ based on the weight of S. First reported in the 1960s,[5] the conventional Na-S battery comprises molten sodium metal negative electrode and molten sulfur positive electrode separated by a β”-alumina solid electrolyte (BASE) ceramic, which not only facilitates the conduction of Na^+ but also tightly separates molten electrodes to eliminate self-discharge. To ensure the sufficient reactivity necessary for the optimal utilization of the S and the emergent polysulfide species (Na_2S_x, $x \geq 3$), typical operations are conducted at high temperatures (HT) above 300 °C to maintain their liquid states. Further, subtler thermal management is also employed to fully exploit the Joule heat emitted during charge and discharge to maintain the high operating temperatures and maximize energy efficiency.[6,7]

Despite the efforts to maintain the liquid state of the positive electrodes, Na_2S_2 and Na_2S polysulfides formed during battery operations have higher melting points (470 and 1168 °C, respectively)[8] which causes them to precipitate and form electrical insulators that inhibit electrochemical performance (e.g., the capacity is limited to 557 mAh (g-S)$^{-1}$ and a specific energy density of 760 Wh kg^{-1} corresponding to the formation of liquified Na_2S_x, x = 3.).[9] Furthermore, HT Na-S batteries are also susceptible to corrosion and explosion, which not only

makes the selection of cell components such as the current collectors and sealants extremely challenging, but also plagues the system with safety issues and high maintenance costs.[10,11]

As a strategy to combat the issues associated with HT operations, Na-S batteries capable of room temperature (RT) operations have been proposed. Although the BASE exhibits a sufficient ionic conductivity for room-temperature operation Na-S batteries,[12–14] the high resistance resulting from its thickness and interfacial behavior lead to poor kinetics. Reducing the operation temperatures also limits the electrochemical performance of RT Na-S batteries because of the formation of solid polysulfides with sluggish electrochemical reactivity. As alternatives, gel polymers[15–17] and organic electrolytes[18–20] have been reported by a number of studies attempting to enhance the reactivities of the electrochemically dormant species. Nonetheless, the utilization of these alternatives has been found to pose some impediments to RT operations. For instance, i) in the absence of the BASE, the intermediate species which are highly soluble in the liquid electrolytes, easily migrate to the negative electrode (so-called "shuttle effect"), resulting in diminished capacity and poor cycling performance;[21] ii) the growth of Na metal dendrites during charging makes the battery prone to short-circuiting;[22] and iii) when conventional organic electrolytes are employed, their insufficient thermal and chemical stabilities cause safety-related issues coupled with cell performance degradation.[23,24]

In a bid to circumvent the above-mentioned challenges, intermediate-temperature (IT, *ca.*150 °C) Na-S batteries that use both BASE and liquid electrolytes have also been explored (the electrochemical properties of intermediate-temperature Na-S batteries are summarized in Table S1 in the Supporting Information).[25–30] The BASE is known to manifest a high ionic conductivity at IT (50 mS cm^{-1} at 150 °C), making them uniquely applicable for Na-S batteries for their ability to prohibit polysulfides migration.[29,31,32] The liquid electrolyte, which is introduced in the positive electrode compartment, enhances the reactivity of polysulfide electrode materials, thus improving their utilization. Although research on IT Na-S batteries is

still in its incipient stages, the availability of a wider variety of materials, such as some polymers suitable as IT cell components, makes them more promising than their HT counterparts.[10,33]

Even so, the fragility of BASE is still challenging for the application of HT and IT system. Once the BASE is broken, the direct contact of molten Na and S might cause inherently violent reaction, potentially leading to fire and even explosion.[10,33] Hence, more attention should be paid to thermal and electrochemical stabilities of the liquid electrolytes, because organic electrolytes used at RT may cause some safety issues in such extreme conditions. In connection to the safey concern of IT operations, ionic liquids (ILs or molten salts), entirely made of ions have emerged as propitious candidates for Na-S as well as analogous Li-S battery systems,[34–36] due to their unique properties such as low flammability, low volatility, and high thermal stability.[37–39] Particularly, ILs entirely composed of alkali metal cations (inorganic ILs) not only exhibit higher thermal stability than those with organic cations,[40,41] but their conductivities and wide electrochemical windows are also sufficiently high for energy device applications.[42–44]

In this work, a new type of IT Na-S battery, which utilizes a dual electrolyte composed of BASE and Na[OTf]-Cs[TFSA] ($[OTf]^-$ = trifluoromethanesulfonate and $[TFSA]^-$ = bis(trifluoromethanesulfonyl)amide) IL is proposed. The IL, which is placed in the positive electrode compartment, enhances the reactivities of the S and polysulfide active materials, thereby improving their utilization and consequently the energy density of the battery. In the proposed system, we select an IL incorporating the $[OTf]^-$ counteranion due to its high solvation properties, particularly for polysulfides, boosting kinetic performance as has been reported for Na-S batteries and analogous Li-S batteries utilizing $[OTf]^-$-based organic electrolytes[12–14,45–48] and IL electrolytes[34]. However, this strategy of enhancing the solubility of intermediate polysulfide species also tends to shorten cycling lifetimes because of the simultaneously heightened polysulfide shuttling.[46] Thus, we adopt the BASE, a selective Na^+ conductor, to eliminate the polysulfide shuttle effect and enhance the cycle life. Moreover, we discuss the

thermal behavior and physicochemical properties and electrochemical window of the Na[OTf]-Cs[TFSA] system, reliability of the Na metal deposition-dissolution process on BASE, and charge-discharge performance of the Na/S cell at intermediate temperatures. The proposed dual electrolyte system confers advantages, such as vigorous kinetics and outstanding cycle life seen in HT systems while achieving a higher capacity via elevating S utilization.

2. Result and Discussion

As illustrated in **Figure 1**, this study proposes an IT Na-S battery in which a BASE disc is used to separate the liquified sodium metal negative electrode compartment from the positive electrode compartment consisting of an IL, S, and a carbon current collector. During discharge, the Na metal in the negative electrode compartment is oxidized to Na^+, which migrates through the BASE to the positive electrode compartment where S is reduced to polysulfide anions to form Na_2S_x. When voltage is applied during charging, the polysulfide anions are oxidized to S, liberating Na^+ to migrate back to the negative electrode compartment through BASE for reduction into Na metal. Although practical cells can be both flat or tubular, the present experimental setup employs a flat cell structure in order to pressurize the interface between liquified Na metal and BASE, thereby establishing homogeneous reaction sites. This approach is taken on account of the poor wettability of Na to the BASE, which would likely lead to inhomogeneous reactivities in the positive electrode compartment (Figure S1, Supporting Information).[32,49,50] Details regarding the preparation and description of the cell are furnished in the Experimental section.

As a strategy for enhancing the kinetics of inert polysulfides, an electrolyte based on Na[OTf] is adopted as the medium for Na^+ conduction. Due to the high donor number of $[OTf]^-$ (compared to typical counter anions such as $[BF_4]^-$ and $[TFSA]^-$), it is postulated to promote the dissolution of polysulfides into the electrolyte,[12–14,34,45–48] thereby improving the electrochemical performance. However, alkali metal OTf salts tend to have high melting points

above 150 °C because of the low degree of freedom in the anionic structure.[43] Thus, in order to reduce the melting point of the electrolyte, the Na[OTf] was combined with Cs[TFSA], which has a melting point of 127 °C (Table S2, Supporting Information) through the effect of Gibbs energy of mixing.[42,51] Accordingly, the host electrolyte for the IT Na-S battery proposed in this study embodies a binary IL system consisting of Na[OTf]-Cs[TFSA].

In order to determine the appropriate molar ratio of the Na[OTf]-Cs[TFSA] system with a melting point suitable for IT Na-S operations, the endothermic transition temperatures for molar ratios in the x(Na[OTf]) range of 0 to 0.7 (x(Na[OTf]) = Na[OTf] fraction = n(Na[OTf]) / {n(Na[OTf]) + n(Cs[TFSA])} in the initial state, where n denotes molar number) were obtained through differential scanning calorimetry (DSC) as shown in **Figure 2a** (see Figure S2 and Table S2 for the corresponding DSC data, Supporting Information). Across all molar ratios of the Na[OTf]-Cs[TFSA] system, the DSC curves appear considerably complicated due to the emergence of several endothermic peaks, which made the identification of each solid phase difficult. This observation is attributed to the emergence of metastable phases during cooling, as suggested by previous DSC studies on sulfonylamide salts.[52–54] Nevertheless, the liquidus lines of the salts were clearly determined through the DSC analysis and further affirmed by visual confirmation of melting occurring above the melting points. The melting temperature was observed to decrease to the eutectic point of 120 °C around the molar ratio of x(Na[OTf]) = 0.05, attesting the suitability of this IL for relatively low temperature operations.

The Na^+ ion conductivity was investigated using a moderate x(Na[OTf]) of 0.2, whose low melting point of 129 °C was deemed sufficient for supporting a liquidus environment at IT. **Figure 2b** compares the ionic conductivity of the Na[OTf]-Cs[TFSA] IL at x(Na[OTf]) = 0.2 with those for organic and IL electrolytes for Na secondary batteries.[29,44,55–62] The data pertaining to the conductivity of BASE was obtained from a previous report on the same material.[29] The Na[OTf]-Cs[TFSA] (x(Na[OTf]) = 0.2) IL manifested a high conductivity of 8.6 mS cm^{-1} at 150 °C (which is comparable or higher than those of conventional organic and

IL electrolytes at RT). Viscosity (η) of the Na[OTf]-Cs[TFSA] (x(Na[OTf]) = 0.2) IL is shown in **Figure 2c** and its temperature dependence is fitted with the Vogel–Tammann–Fulcher (VTF) equation (Table S4).[63–65] The viscosity of the IL is 59.1 mPa s at 150 °C and is comparable with those of TFSA-based inorganic ILs. [66] The density of the Na[OTf]-Cs[TFSA] (x(Na[OTf]) = 0.2) IL at 150 °C was determined to be 2.1 g cm^{-3}.

Electrochemical window defined by the cathodic and anodic limits is an important indicator to judge the compatibility of an electrolyte with electrode materials. The cyclic voltamnetry (CV) measurements were conducted for the Na[OTf]-Cs[TFSA] (x(Na[OTf]) = 0.2) IL using Al working electrodes for anodic and cathodic scan and a Pt working electrode for anodic scan at a scan rate of 5 mV s^{-1}. The combined CV curves are shown in **Figure 2d**. A reversible Na metal deposition-dissolution occurs at 0 V vs. Na^+/Na. A rapid increase of the current at 5.1 V at the Pt working electrode shows the anodic limit of the IL, which corresponds to the oxidation of the anions. The IL exhibits a relatively high electrochemical window of 5.1 V, demonstrating excellent stability as an electrolyte for sodium secondary batteries at intermediate temperatures. There is no significant anodic current observed at the Al electrode due to the formation of robust passivation layer, indicating the Al corrosion has not been observed with the electrolyte, which is also consistent with the suppressed Al corrosion problem in organic ILs.[67]

The thermal stability of the Na[OTf]-Cs[TFSA] IL was examined through thermogravimetry analysis, as illustrated in Figure S3, Supporting Information. The electrolyte manifests negligible mass loss at temperatures below 400 °C, showing high thermal stability that is beneficial for Na/S IT operations. Further, a heating test was performed to confirm the chemical stability of the Na[OTf]-Cs[TFSA] IL when in contact with active materials (S and Na_2S_4, an intermediate polysulfide) at 150 °C. The S and Na_2S_4 were added into the Na[OTf]-Cs[TFSA] IL at 150 °C in the weight ratio of S/IL = 1.0 % and Na_2S_4/IL = 1.4 % and constantly stirred for varying periods of time. For comparison, similar tests were conducted on an organic cation IL, Na[OTf]-[C_4C_1pyrr][OTf] (x(Na[OTf]) = 0.2) ([C_4C_1pyrr]$^+$ = *N*-butyl-*N*-

methylpyrrolidinium). As visualized in Figure S4, Supporting Information, after continuous heating for 100 min, the colors of the S/Na[OTf]-Cs[TFSA] and Na_2S_4/Na[OTf]-Cs[TFSA] mixtures are observed to change to yellow and dark orange, respectively; evincing the partial dissolution of S and Na_2S_4 in conformity with previous reports.[68] However, in the case of S and Na_2S_4 in the organic IL, drastic changes in appearance, characterized by a dark brown solution and volatile decomposed materials deposited on the top of the test bottles, were observed. For verification, a blank test involving pure Na[OTf]-[C_4C_1pyrr][OTf] was performed. No color changes nor sign of decomposition were seen, suggesting that the previously observed decomposition of the organic IL was due to the presence of S or Na_2S_4. These observations are a further attestation to the superior chemical stability of the Na[OTf]-Cs[TFSA] IL for IT Na-S batteries compared to the systems with organic species such as the Na[OTf]-[C_4C_1pyrr][OTf] IL at 150 °C.

For further scrutiny into other aspects of the proposed Na-S battery, a Na metal deposition-dissolution test was performed to discern the Na metal negative electrode performance and confirm the reliability of the flat cell. A Na/BASE/Na symmetric cell was constructed at 150 °C in the same configuration as a Na/S cell but with both the positive and negative electrode compartments separately filled with liquified Na metal (electrode area: 0.785 cm^2). Alternating galvanostatic Na metal deposition-dissolution measurements were conducted for 400 cycles over 160 h, with the period of each cycle fixed at 0.4 h. The currents were increased in a stepwisely fashion after every 100 cycles as shown in **Figure 3a**. As shown in the voltage profiles, the Na/BASE/Na cell manifests stable Na metal deposition-dissolution marked by constant overpotentials of about 7 mV, 15 mV, 27 mV, and 50 mV observed at 0.2 mA (**Figure 3b**), 0.5 mA (**Figure 3c**), 1.0 mA (**Figure 3d**), and 2.0 mA (**Figure 3e**), respectively, throughout the cycling. Electrochemical impedance spectroscopy was carried out in the initial state and after every 100 cycles, as shown by the Nyquist plots in **Figure 3f**. Here, no significant changes in the interfacial resistance corresponding to the semicircles were noted throughout the

400 cycles. This result indicates the BASE can protect liquified Na metal chemically and physically without forming dendrite. The bulk resistance was seen to continually decrease during the initial 300 cycles; an indication of the progressive improvements occurring in the Na/BASE interface with continued cycling. The relatively large bulk resistances considering the operating temperature and conductivity of the BASE is due to the small contact area (0.785 cm^2) and thickness (1 mm) of the BASE.

Following the validation of the Na[OTf]-Cs[TFSA] (x(Na[OTf]) = 0.2) IL electrolyte and the confirmation of stable Na metal deposition-dissolution at the Na/BASE interface, a Na/S cell comprising the dual BASE/IL electrolyte was assembled for further electrochemical performance tests. Charge-discharge tests were performed at 150 °C at the current of 0.1 mA, as shown in **Figure 4a**. Even at 150 °C, where the Na_2S_x, $x \leq 5$, compounds are solid,[8] a high initial discharge capacity of 795 mAh $(g\text{-}S)^{-1}$, almost equivalent to the theoretical capacity of Na_2S_2, was achieved. The voltage profiles are divided into four regions by blue dashed lines that indicate the theoretical capacities of different polysulfides (Na_2S_x, x = 8, 6, 5, 4, 3, and 2). In Region I, a gentle plateau that appears above *ca.* 2.1 V and ends at the theoretical capacity at x = 6 was observed. The sloping Region II, which corresponds to x = 5 and 4, was seen in the 2.1–1.9 V range. Region III is characterized by a small plateau associated with x = 3 around 1.9 V. Continued discharge below 1.9 V in Region IV coresponds to x = 2 followed by a rapid voltage drop to the cut-off voltage. The charge profile also reveals the good reversibility of the proposed Na/S cell by providing an initial charge capacity of 770 mAh $(g\text{-}S)^{-1}$. The voltage variation visualized here conforms with previously reported profiles of IT and RT Na-S batteries at low rates.[4,26,28,69]

For a deeper insight into the electrochemical performance of the proposed cell, discharge and charge profiles were obtained at varying currents in the sequence 0.1 mA, 0.2 mA, 0.5 mA, 1.0 mA, and 2.0 mA (**Figure 4b**), along with the rate capability plot shown in **Figure 4c**. At voltages above 1.9 V (corresponding discharge capacity of *ca*. 400 mAh $(g\text{-}S)^{-1}$), the proposed

cell showed good consistency across the different currents tested due to the facile conversion of high order polysulfides (Na_2S_x where $x \geq 4$). However, below 1.9 V, the capacity was found to decrease at high currents owing to the low electrochemical reactivities of the polysulfides formed at low voltages (Na_2S_x where $x < 4$). The capacity loss above *ca*. 400 mAh $(g\text{-}S)^{-1}$ at high currents can be further rationalized by the low solubility of the corresponding polysulfides in the IL, which also matches the large hysteresis observed in the low-voltage region of the charge-discharge profile (**Figure 4a**). A complemental demonstration by plotting the differential capacity vs voltage (dQ/dV) curves are shown in Figure S5, Supporting Information. It is clear that there are several peaks below 1.9 V in the discharge curves at lower rate, indicating the formation of Na_2S_x with $x \geq 4$ (Figure S5a–c, Supporting Information). On the other hand, these peaks gradually fade or disappear with increasing rate (Figure S5d–e, Supporting Information), which is attributed to the poor electrochemical reactivity of the Na_2S_x with $x < 4$. Similar observations wherein the behavior of polysulfides is contingent on the voltage regions have also been reported in an RT Na-S battery.[13]

To establish the long-term performance of the proposed Na/S cell, charge-discharge tests were conducted over 1000 cycles at 0.5 mA, as shown in the charge-discharge profiles (**Figure 4d**) and the cycle performance plot (**Figure 4e**). Here, the capacities above 1.9 V are considered as the main capacities at this current (**Figure 4d**). Throughout the 1000 cycles, the dual BASE/IL electrolyte demonstrates a stable performance, attaining a high cycleability with an average capacity of 381 mAh $(g\text{-}S)^{-1}$ and an average coulombic efficiency of 100 %. It is worth mentioning that such long and stable cycles have never been reported for similar types of IT Na/S cells. During the initial 50 cycles, a gradual increase in capacity ascribed to the improvement of the S and sulfide electrochemical reactions in the active sites during cycling is seen. As discussed earlier, the discharge profiles for voltages above 1.9 V appear to overlap throughout the cycling, indicating the high reversibility of the reactions involving the formation of Na_2S_x with $x \geq 4$. Judging from the charge-discharge profiles, the poor electrochemical

reactivity of the Na_2S_x with $x < 4$ seems to be one of the underlying reasons for the random fluctuation of capacity observed after 150 cycles. Therefore, to improve the rate performance of this system, further investigation and modification is required to enhance the kinetics of the phases formed below 1.9 V.

For a deeper understanding of the results obtained in this study, in particular, the effect of $[OTf]^-$ counter anion on the charge-discharge behavior, a control charge-discharge experiment was conducted on an IL electrolyte exclusively made of the TFSA anion for comparison with the Na[TFSA]-Cs[TFSA] (x(Na[TFSA]) = 0.2) IL under the same conditions. The Na[TFSA]-Cs[TFSA] IL achieved a limited reversible capacity (below 80 mAh $(g\text{-}S)^{-1}$) at 0.1 and 0.2 mA (Figure S6 and S7, Supporting Information), despite showing good cycleability at 0.5 mA (the capacity constantly increases) (Figure S8 and S9, Supporting Information). The electrochemical performance improvement in the Na[OTf]-Cs[TFSA] (x(Na[OTf]) = 0.2) should be correlated with better compatibility of Na_2S_x in the system than the Na[TFSA]-Cs[TFSA] (x(Na[TFSA]) = 0.2) IL. The difference in chemical stability and solubility of Na_2S_x seems to be related to it, but further experimental results are required to fully clarify this point (see Figure S10, Supporting Information, for preliminary tests on chemical stability and solubility).

Based on the previously discussed chemical stability results, this study not only demonstrates the use of organic compounds as an impediment to high IL electrolyte stability but also establishes the introduction of $[OTf]^-$ into the electrolyte as an expedient means to enhance the utilization of S and Na_2S_x. The results further validate the use of the inorganic Na[OTf]-Cs[TFSA] IL as an effective strategy for achieving stable cycling in a high-performance IT Na/S battery.

3. Conclusion

In summary, this study presents a novel, dual BASE/Na[OTf]-Cs[TFSA] IL electrolyte, devised for IT Na-S battery operations at 150 °C. The Na[OTf]-Cs[TFSA] IL is found to have vigorous

physicochemical properties, wide electrochemical window of 5.1 V as well as excellent thermal and chemical stability, making it a suitable component for the proposed dual electrolyte system. The reliability of BASE in a solid-liquid hybrid flat cell was validated through deposition-dissolution tests performed on a symmetric Na/BASE/Na cell for 400 cycles. The proposed dual combination not only prevents the polysulfide shuttle effect through the selective Na^+ conduction by the BASE, but it also enhances the positive electrode reactivity through the IL. Accordingly, the IT Na-S battery achieves a high reversible capacity of 795 mAh $(g\text{-}S)^{-1}$, manifesting a remarkable utilization of S at 0.1 mA (electrode area: 0.785 cm^2). In a long cycle test, an average capacity of 381 mAh $(g\text{-}S)^{-1}$ and an average coulombic efficiency of 100% are achieved over 1000 cycles at 0.5 mA. It is worth noting that the proposed IT Na-S system is still at its incipient stage, and therefore significant improvements in performance are to be expected with further optimization of the cell construction as well as the IL structure or composition (e.g., enhancing the solvation of polysulfides in electrolyte and avoidance of Cs). In this study, the energy density is unsatisfactory as 20.6 Wh L^{-1} based on the volume of S, IL, carbon lead, and BASE due to the limited S content. Meanwhile, the poor utilization of Na_2S_x ($x < 4$) caused by sluggish kinetics below 1.9 V as a major limitation to achieving a good capacity. As such, for the realization of these IT Na-S batteries, further exploration into enhancing the reactivities of such polysulfides as well as investigations into the interfacial mechanisms involving the active material, IL, and carbon lead at the positive electrode, would be necessary.

4. Experimental Section

Apparatus and materials

Volatile materials were handled in a vacuum line constructed using stainless steel, Pyrex glass, poly(tetrafluoroethylene) (PTFE), and poly(tetrafluoroethylene-co-perfluoro(alkylvinyl)ether) (PFA). Nonvolatile materials were handled under a dry Ar atmosphere in a glove box ($H_2O <$

1 ppm, O_2 < 1 ppm)). Sulfur (Wako Pure Chemical, purity > 98.0 %) was dried in a PFA container at 120 °C under vacuum for one day. The upper part of the container was cooled with a fan to prevent sublimation outside the container. Sodium disulfide (Wako Pure Chemical, purity > 98.0 %) was dried at 100 °C under vacuum for one day and ground into powder prior to use. Sodium tetrasulfide was used as supplied (Dojindo, purity ≦ 100 %) or prepared by the stoichiometric reaction Na_2S and S. Sodium trisulfide (Dojindo, purity ≦ 100 %) was used as received.

The electrolytes, Na[OTf] (Sigma-Aldrich, purity > 98 %), Na[TFSA] (Kishida Chemical, purity > 99.0 %), and [C_4C_1pyrr][OTf] (Iolitec, purity > 99 %), were dried under vacuum at 100 °C for 3 days. The Cs[TFSA] salt (Morita Chemical, purity > 99.0 %) was dissolved in anhydrous ethanol to form a saturated solution which was then recrystallized by adding an equal volume of trifluorotoluene acting as the lean solvent. The resulting white solid was dried under vacuum at 100 °C for 3 days. Carbon paper (Toray, TGP-H-120) and β”-alumina solid electrolyte (BASE) (Ionotec, 24 mm in diameter, 1 mm in thickness) were dried at 300 °C under vacuum for 3 days.

Electrolyte and analysis

To prepare the IL electrolyte, the component salts were mixed in the target molar ratios, heated above their melting points, and constantly stirred to obtain a homogeneous mixture.

The phase transition temperatures of the Na[OTf]-Cs[TFSA] binary systems were determined by differential scanning calorimetry (DSC; Hitachi High-Technologies, DSC220) at a scan rate of 2 K min^{-1} under a dry N_2 atmosphere. The DSC samples were sealed in Al cells under a dry Ar atmosphere. The thermal stability of the Na[OTf]-Cs[TFSA] (x(Na[OTf]) = 0.2) salt was measured by thermogravimetric analysis (Rigaku, Thermo plus EVO, TG 8120) at a scan rate of 5 K min^{-1} under a dry Ar atmosphere. The ionic conductivity of the Na[OTf]-

Cs[TFSA] (x(Na[OTf]) = 0.2) salt was measured using an AC impedance technique where an AC perturbation of 10 mV was applied using an electrochemical analyzer (Hokuto Denko, HZ-Pro). The sample was sealed in a cell with two Pt black electrodes (Radiometer Analytical), whose cell constant was calibrated using the KCl standard solution. Viscosity was measured using a digital viscometer (Brookfield Engineering Laboratories, DV1MLVTJ0+HT-110115ADP).

Electrochemical stability of the Na[OTf]-Cs[TFSA] (x(Na[OTf]) = 0.2) IL was evaluated by CV measurements at 150 °C in a two-electrode cell using Al and Pt working electrodes and liquid Na metal counter electrode at a scan rate of 5 mV s^{-1}. Density was determined by measuring the volume and mass of the IL in a pycnometer at 150 °C.

Thermal and chemical stabilities of the ILs in the presence of S and Na_2S_4 were confirmed through visual observation. Elemental S and Na_2S_4 were separately added into glass vials containing the Na[OTf]-Cs[TFSA] (x(Na[OTf]) = 0.2) and Na[OTf]-[C_4C_1pyrr][OTf] (x(Na[OTf]) = 0.2) ILs at the weight ratios of 5 mg/500 mg and 7 mg/500 mg for the S/IL and Na_2S_4/IL, respectively. The vials were tightly sealed in Ar-filled glove box and heated outside to 150 °C under constant stirring. A blank Na[OTf]-[C_4C_1pyrr][OTf] IL was heated under the same conditions for comparison.

The stability and solubility were visually confirmed using Na_2S_4 or Na_2S_3 (Na_2S_3 is considered as a mixture of Na_2S_4 and Na_2S_2) in the ILs at 150 °C. The polysulfides, Na_2S_4 and Na_2S_3, were added into test tubes with the Na[OTf]-Cs[TFSA] (x(Na[OTf]) = 0.2) and Na[TFSA]-Cs[TFSA] (x(Na[TFSA]) = 0.2) ILs at the weight ratios of 1.36 mg/2000 mg and 1.48 mg/2000 mg for the Na_2S_4/IL and Na_2S_3/IL, respectively. The test tube was tightly sealed in the Ar-filled glove box and heated at 150 °C for 5 days.

Cell preparation and electrochemical measurements

In the stringently airtight flat cell shown in Figure S1 in the Supporting Information, a BASE disc is placed at the center to separate the negative and positive electrode compartments (area: 0.785 cm^2, diameter: 1.00 cm, thickness 1.0 mm). The negative electrode compartment, completely filled with Na metal, and the positive electrode compartment, filled with a mixture of conductive carbon, S, and IL, were packed by pressing the electrodes with springs from both sides.

The Na/BASE/Na symmetric cell was constructed in the same manner as the Na/S cell at 150 °C. Sodium metal (*ca.* 100 mg) was placed in both the positive and negative electrode compartments. The electrochemical measurements were carried out with the aid of an electrochemical measurement system (BioLogic, VSP). Galvanostatic Na deposition-dissolution measurements were conducted with the period of each cycle fixed to 0.4 h. The current was increased progressively after every 100 cycles in the sequence of 0.2 mA, 0.5 mA, 1.0 mA, and 2.0 mA. Electrochemical impedance spectroscopy was carried out in the initial state and after 100, 200, 300, and 400 cycles at a frequency range of 10 mHz–1 MHz and an AC amplitude of 10 mV.

The galvanostatic charge-discharge behavior of the Na/S cell with the dual BASE/IL electrolyte was evaluated at 150 °C. Carbon paper punched into five discs with diameters of 1 cm were impregnated with the ILs under vacuum at 150 °C prior to measurements. S powder and the carbon/electrolyte composite were directly added into the positive electrode compartment (typically 3 mg S in 300 mg IL, corresponding to 0.66 mol S per 1 dm^3 IL (0.31 mol kg^{-1}) based on the density of IL at 150 °C). Excessive amounts of Na metal (*ca.* 100 mg) were used for the negative electrode. After the assembly, the cell was heated to 150 °C for 12 h to establish the temperature equilibrium. Cut-off voltages were set to the 1.2 V - 2.8 V range, while the currents were varied at 0.1 mA, 0.2 mA, 0.5 mA, 1.0 mA, and 2.0 mA. The specific capacity was calculated based on the weight of active S. Because the Na/S cell was fully charged in the initial state, the coulombic efficiency was defined as (cycle n+1 discharge

capacity)/(cycle *n* charge capacity). All the cells involved in the experiments were assembled and measured in the Ar-filled glove box.

Supporting Information ((delete if not applicable))
Supporting Information is available from the Wiley Online Library or from the author.

Acknowledgements
This study was partly supported by the Japanese Ministry of Education, Culture, Sports, Science and Technology (MEXT) program "Elements Strategy Initiative to Form Core Research Center" (JPMXP0112101003) and JSPS KAKENHI Grant Number JP21H02047. One of the authors, Di Wang, thanks the China Scholarship Council (CSC) for the financial support.

Received: ((will be filled in by the editorial staff))
Revised: ((will be filled in by the editorial staff))
Published online: ((will be filled in by the editorial staff))

References

[1] International Energy Agency, *World energy balances 2020: Overview*, IEA, Paris **2020**.

[2] N. L. Panwar, S. C. Kaushik, S. Kothari, *Renew. Sustain. Energy Rev.* **2011**, *15*, 1513.

[3] B. Dunn, H. Kamath, J.-M. Tarascon, *Science* **2011**, *334*, 928.

[4] T. Oshima, M. Kajita, A. Okuno, *Int. J. Appl. Ceram. Technol.* **2004**, *1*, 269.

[5] J. T. Kummer, N. Weber, *SAE Trans.* **1968**, *76*, 1003.

[6] R. Okuyama, E. Nomura, *J. Power Sources* **1999**, *77*, 164.

[7] J. K. Min, C.-H. Lee, *J. Power Sources* **2012**, *210*, 101.

[8] J. Sangster, A. D. Pelton, *J. Phase Equilibria* **1997**, *18*, 89.

[9] K. B. Hueso, M. Armand, T. Rojo, *Energy Environ. Sci.* **2013**, *6*, 734.

[10] Z. Wen, Y. Hu, X. Wu, J. Han, Z. Gu, *Adv. Funct. Mater.* **2013**, *23*, 1005.

[11] X. Lu, G. Xia, J. P. Lemmon, Z. Yang, *J. Power Sources* **2010**, *195*, 2431.

[12] S. Wenzel, H. Metelmann, C. Raiß, A. K. Dürr, J. Janek, P. Adelhelm, *J. Power Sources* **2013**, *243*, 758.

[13] I. Kim, J.-Y. Park, C. H. Kim, J.-W. Park, J.-P. Ahn, J.-H. Ahn, K.-W. Kim, H.-J. Ahn, *J. Power Sources* **2016**, *301*, 332.

[14] L. Medenbach, P. Hartmann, J. Janek, T. Stettner, A. Balducci, C. Dirksen, M. Schulz, M. Stelter, P. Adelhelm, *Energy Technol.* **2020**, *8*, 1901200.

[15]C.-W. Park, J.-H. Ahn, H.-S. Ryu, K.-W. Kim, H.-J. Ahn, *Electrochem. Solid State Lett.* **2006**, *9*, A123.

[16]C.-W. Park, H.-S. Ryu, K.-W. Kim, J.-H. Ahn, J.-Y. Lee, H.-J. Ahn, *J. Power Sources* **2007**, *165*, 450.

[17]D. Kumar, Mohd. Suleman, S. A. Hashmi, *Solid State Ionics* **2011**, *202*, 45.

[18]H. Ryu, T. Kim, K. Kim, J.-H. Ahn, T. Nam, G. Wang, H.-J. Ahn, *J. Power Sources* **2011**, *196*, 5186.

[19]Y.-M. Chen, W. Liang, S. Li, F. Zou, S. M. Bhaway, Z. Qiang, M. Gao, B. D. Vogt, Y. Zhu, *J. Mater. Chem. A* **2016**, *4*, 12471.

[20]R. Carter, L. Oakes, A. Douglas, N. Muralidharan, A. P. Cohn, C. L. Pint, *Nano Lett.* **2017**, *17*, 1863.

[21]Y.-X. Wang, W.-H. Lai, S.-L. Chou, H.-K. Liu, S.-X. Dou, *Adv. Mater.* **2020**, *32*, 1903952.

[22]X. Hong, J. Mei, L. Wen, Y. Tong, A. J. Vasileff, L. Wang, J. Liang, Z. Sun, S. X. Dou, *Adv. Mater.* **2019**, *31*, 1802822.

[23]C. Arbizzani, G. Gabrielli, M. Mastragostino, *J. Power Sources* **2011**, *196*, 4801.

[24]T. Yim, M.-S. Park, J.-S. Yu, K. J. Kim, K. Y. Im, J.-H. Kim, G. Jeong, Y. N. Jo, S.-G. Woo, K. S. Kang, I. Lee, Y.-J. Kim, *Electrochim. Acta* **2013**, *107*, 454.

[25]K. M. Abraham, R. D. Rauh, S. B. Brummer, *Electrochim. Acta* **1978**, *23*, 501.

[26]X. Lu, B. W. Kirby, W. Xu, G. Li, J. Y. Kim, J. P. Lemmon, V. L. Sprenkle, Z. Yang, *Energy Environ. Sci* **2013**, *6*, 299.

[27]X. Lu, G. Li, J. Y. Kim, D. Mei, J. P. Lemmon, V. L. Sprenkle, J. Liu, *Nat. Commun.* **2014**, *5*, 4578.

[28]F. Yang, S. M. A. Mousavie, T. K. Oh, T. Yang, Y. Lu, C. Farley, R. J. Bodnar, L. Niu, R. Qiao, Z. Li, *Adv. Energy Mater.* **2018**, *8*, 1701991.

[29]G. Nikiforidis, G. J. Jongerden, E. F. Jongerden, M. C. M. van de Sanden, M. N. Tsampas, *J. Electrochem. Soc.* **2019**, *166*, A135.

[30] S. Kandhasamy, G. Nikiforidis, G. J. Jongerden, F. Jongerden, M. C. M. Sanden, M. N. Tsampas, *ChemElectroChem* **2021**, *8*, 1156.

[31] K. . Ahlbrecht, C. Bucharsky, M. Holzapfel, J. Tübke, M. J. Hoffmann, *Ionics* **2017**, *23*, 1319.

[32] Y. Wang, D. Zhou, V. Palomares, D. Shanmukaraj, B. Sun, X. Tang, C. Wang, M. Armand, T. Rojo, G. Wang, *Energy Environ. Sci.* **2020**, *13*, 3848.

[33] M.-T. F. Rodrigues, G. Babu, H. Gullapalli, K. Kalaga, F. N. Sayed, K. Kato, J. Joyner, P. M. Ajayan, *Nat. Energy* **2017**, *2*, 1.

[34] J.-W. Park, K. Ueno, N. Tachikawa, K. Dokko, M. Watanabe, *J. Phys. Chem. C* **2013**, *117*, 20531.

[35] M. Watanabe, M. L. Thomas, S. Zhang, K. Ueno, T. Yasuda, K. Dokko, *Chem. Rev.* **2017**, *117*, 7190.

[36] K. Matsumoto, J. Hwang, S. Kaushik, C.-Y. Chen, R. Hagiwara, *Energy Environ. Sci.* **2019**, *12*, 3247.

[37] T. Welton, *Chem. Rev.* **1999**, *99*, 2071.

[38] P. Wasserscheid, W. Keim, *Angew. Chem. Int. Ed.* **2000**, *39*, 3772.

[39] R. D. Rogers, K. R. Seddon, *Science* **2003**, *302*, 792.

[40] Z. Lu, L. Yang, Y. Guo, *J. Power Sources* **2006**, *156*, 555.

[41] M. Götz, R. Reimert, S. Bajohr, H. Schnetzer, J. Wimberg, T. J. S. Schubert, *Thermochim. Acta* **2015**, *600*, 82.

[42] R. Hagiwara, K. Tamaki, K. Kubota, T. Goto, T. Nohira, *J. Chem. Eng. Data* **2008**, *53*, 355.

[43] X. Tu, Y. Chu, C. Ma, *Ionics* **2010**, *16*, 81.

[44] T. Nohira, T. Ishibashi, R. Hagiwara, *J. Power Sources* **2012**, *205*, 506.

[45] H. Chu, H. Noh, Y.-J. Kim, S. Yuk, J.-H. Lee, J. Lee, H. Kwack, Y. Kim, D.-K. Yang, H.-T. Kim, *Nat. Commun.* **2019**, *10*, 188.

[46] A. Gupta, A. Bhargav, A. Manthiram, *ACS Energy Lett.* **2020**, 224.

[47] H. Shin, M. Baek, A. Gupta, K. Char, A. Manthiram, J. W. Choi, *Adv. Energy Mater.* **2020**, *10*, 2001456.

[48] A. Gupta, A. Bhargav, J.-P. Jones, R. V. Bugga, A. Manthiram, *Chem. Mater.* **2020**, *32*, 2070.

[49] D. Reed, G. Coffey, E. Mast, N. Canfield, J. Mansurov, X. Lu, V. Sprenkle, *J. Power Sources* **2013**, *227*, 94.

[50] G. Kim, Y.-C. Park, Y. Lee, N. Cho, C.-S. Kim, K. Jung, *J. Power Sources* **2016**, *325*, 238.

[51] J. Hwang, A. N. Sivasengaran, H. Yang, H. Yamamoto, T. Takeuchi, K. Matsumoto, R. Hagiwara, *ACS Appl. Mater. Interfaces* **2021**, *13*, 2538.

[52] K. Matsumoto, T. Oka, T. Nohira, R. Hagiwara, *Inorg. Chem.* **2013**, *52*, 568.

[53] W. A. Henderson, M. Herstedt, Young Victor G., S. Passerini, H. C. De Long, P. C. Trulove, *Inorg. Chem.* **2006**, *45*, 1412.

[54] W. A. Henderson, D. M. Seo, Q. Zhou, P. D. Boyle, J.-H. Shin, H. C. D. Long, P. C. Trulove, S. Passerini, *Adv. Energy Mater.* **2012**, *2*, 1343.

[55] Z. W. Seh, J. Sun, Y. Sun, Y. Cui, *ACS Cent. Sci.* **2015**, *1*, 449.

[56] D.-J. Lee, J.-W. Park, I. Hasa, Y.-K. Sun, B. Scrosati, J. Hassoun, *J. Mater. Chem. A* **2013**, *1*, 5256.

[57] S. Wei, S. Xu, A. Agrawral, S. Choudhury, Y. Lu, Z. Tu, L. Ma, L. A. Archer, *Nat. Commun.* **2016**, *7*, 11722.

[58] D. Zhou, Y. Chen, B. Li, H. Fan, F. Cheng, D. Shanmukaraj, T. Rojo, M. Armand, G. Wang, *Angew. Chem. Int. Ed.* **2018**, *57*, 10168.

[59] K. Matsumoto, T. Hosokawa, T. Nohira, R. Hagiwara, A. Fukunaga, K. Numata, E. Itani, S. Sakai, K. Nitta, S. Inazawa, *J. Power Sources* **2014**, *265*, 36.

[60] D. Monti, E. Jónsson, M. R. Palacín, P. Johansson, *J. Power Sources* **2014**, *245*, 630.

[61] K. Matsumoto, Y. Okamoto, T. Nohira, R. Hagiwara, *J. Phys. Chem. C* **2015**, *119*, 7648.

[62] A. Fukunaga, T. Nohira, Y. Kozawa, R. Hagiwara, S. Sakai, K. Nitta, S. Inazawa, *J. Power Sources* **2012**, *209*, 52.

[63] H. Vogel, *Phys. Z* **1921**, *22*, 645.

[64] G. S. Fulcher, *J. Am. Ceram. Soc.* **1925**, *8*, 339.

[65] W. Xu, E. I. Cooper, C. A. Angell, *J. Phys. Chem. B* **2003**, *107*, 6170.

[66] A. Watarai, K. Kubota, M. Yamagata, T. Goto, T. Nohira, R. Hagiwara, K. Ui, N. Kumagai, *J. Power Sources* **2008**, *183*, 724.

[67] J. Hwang, K. Matsumoto, R. Hagiwara, *Adv. Energy Mater.* **2020**, *10*, 2001880.

[68] G. Nikiforidis, M. C. M. van de Sanden, M. N. Tsampas, *RSC Adv.* **2019**, *9*, 5649.

[69] X. Yu, A. Manthiram, *ChemElectroChem* **2014**, *1*, 1275.

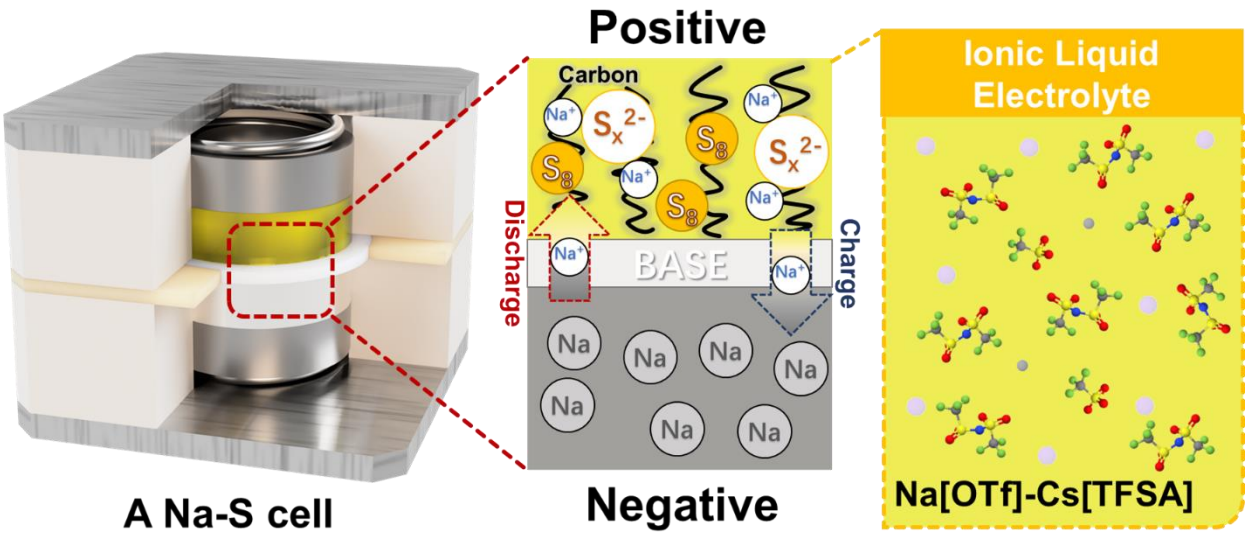

Figure 1. Schematic illustration of the operation mechanisms of the IT Na-S battery employing the dual BASE/IL electrolyte. Operation temperature: 150 °C and IL: Na[OTf]-Cs[TFSA]. The Na^+-conductive BASE impedes the shuttle of S_x^{2-} ions to the negative electrode compartment while the IL facilitates facile electrochemical reactions in the positive electrode compartment.

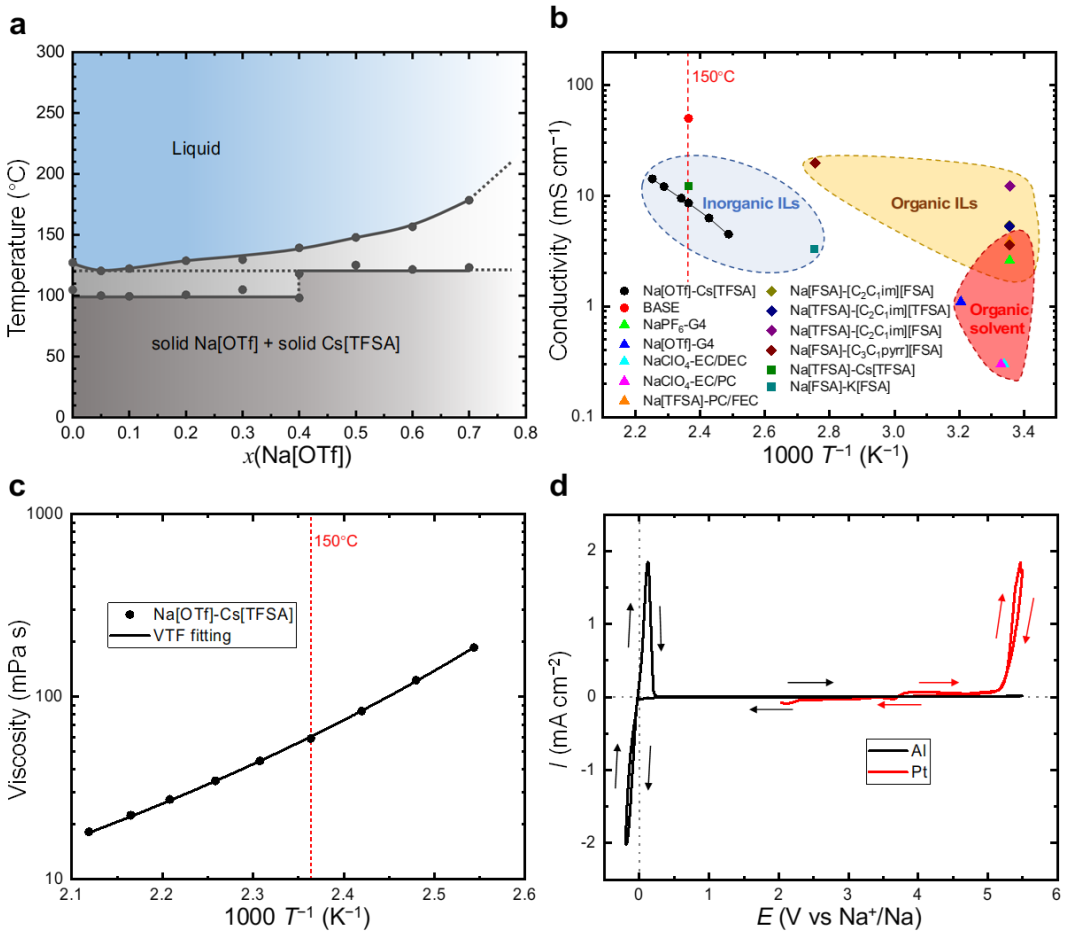

Figure 2. The properties of the Na[OTf]-Cs[TFSA] system. (a) Plots of the major endothermic transition temperatures for molar ratios in the *x*(Na[OTf]) range of 0 to 0.7 derived from the DSC measurements (see Figure S2 and Table S2 for DSC data, Supporting Information). The DSC curves appear complicated, exhibiting multiple transitions arising from the formation of polymorphism and metastable phases, as is typical for sulfonylamide salts.[52–54] (b) A comparison between the ionic conductivity of the Na[OTf]-Cs[TFSA] IL (*x*(Na[OTf]) = 0.2) (black circles) and those of typical electrolytes for Na secondary batteries; (BASE (red circle), common organic electrolytes for Na-S batteries (triangles), organic ILs (diamonds), and other inorganic ILs (squares) (see Table S3 for the conductivity data[29,44,55–62], Supporting Information). (c) Arrhenius plot for the viscosity of the Na[OTf]-Cs[TFSA] IL (*x*(Na[OTf]) = 0.2) and the corresponding VTF (Vogel-Tammann-Fulcher) equation fitting (see Table S4 for the viscosity data and fitting parameters, Supporting Information). (d) Combined CV of the Na[OTf]-Cs[TFSA] IL (*x*(Na[OTf]) = 0.2) at 150 °C. Scan rate: 5 mV s^{-1}.

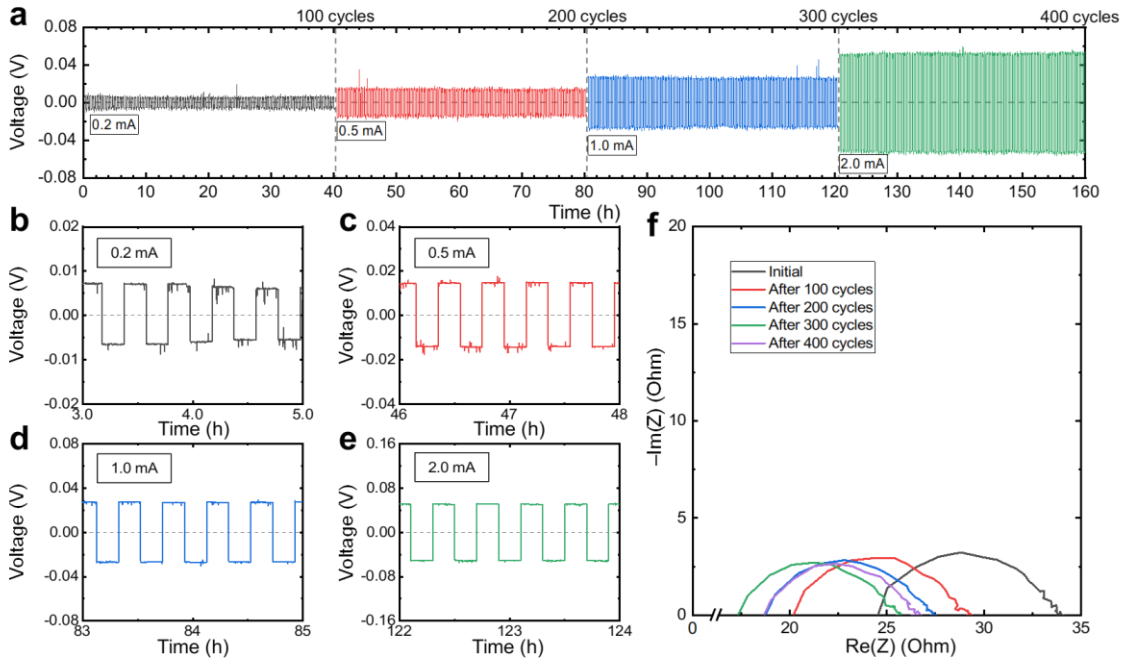

Figure 3. Galvanostatic Na metal deposition-dissolution performance of the Na/BASE/Na symmetric cell (electrode area: 0.785 cm^2) at 150 °C. (a) An overall voltage profile of the symmetric cell during measurement at currents of 0.2 mA, 0.5 mA, 1.0 mA, and 2.0 mA over 400 cycles (0.4 h per cycle). The amount of Na deposited/dissolved per one step is; 0.05, 0.13, 0.25, and 0.51 mAh cm^{-2}, respectively at 0.2 mA, 0.5 mA, 1.0 mA, and 2.0 mA. The magnified voltage profiles for measurements conducted at currents of (b) 0.2 mA, (c) 0.5 mA, (d) 1.0 mA, and (e) 2.0 mA, respectively. (f) The Nyquist plots of the symmetric cell before and after cycling for 0, 100, 200, 300, and 400 cycles. Frequency range: 10 mHz–1 MHz and AC amplitude: 10 mV.

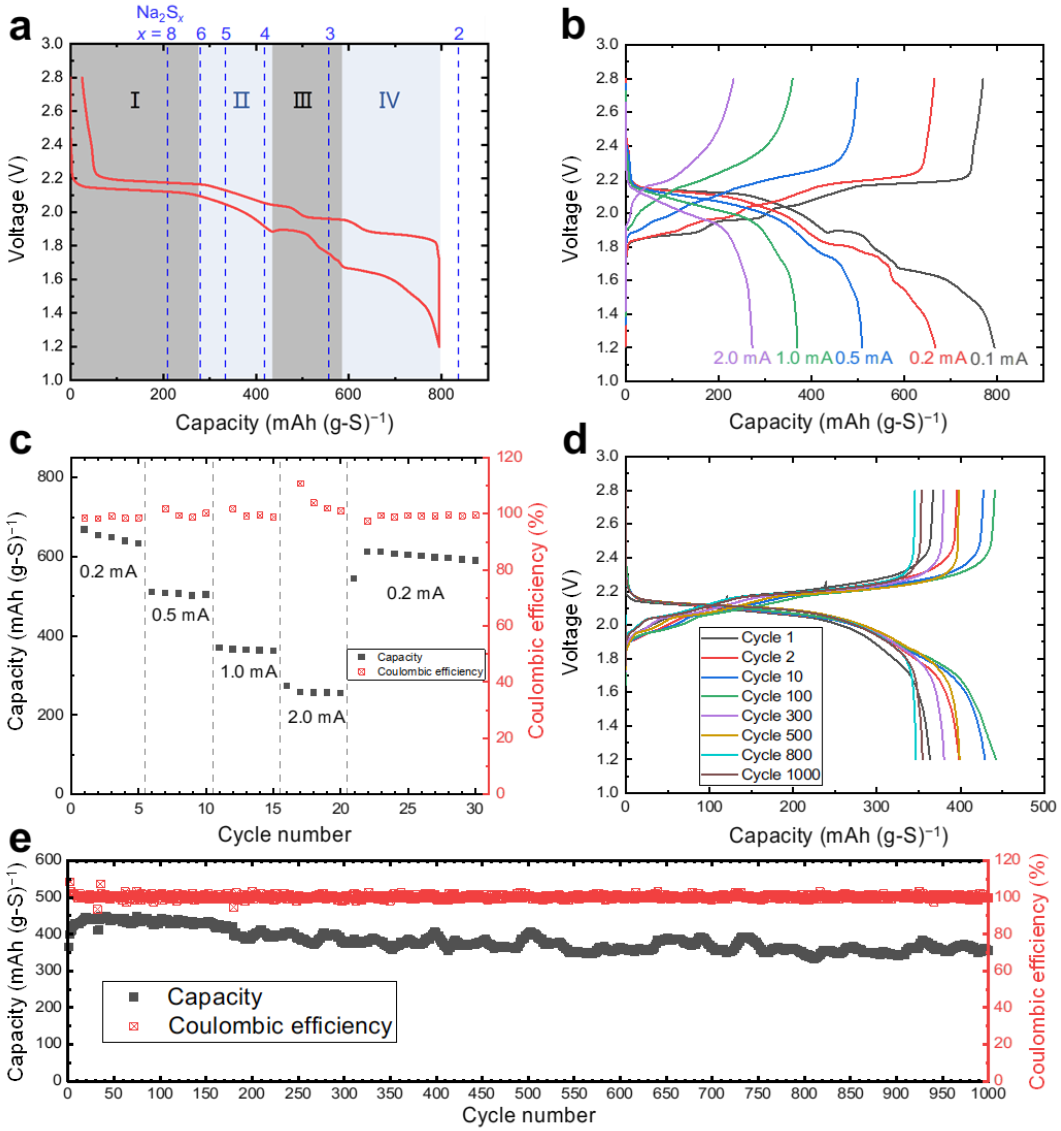

Figure 4. Electrochemical performance of the IT-Na/S cells using the dual BASE/IL electrolyte (IL = Na[OTf]-Cs[TFSA] (*x*(Na[OTf]) = 0.2)) (electrode area: 0.785 cm^2 and temperature: 150 °C). (a) The discharge and charge profile of measurements conducted at 0.1 mA. The blue dashed lines indicate the theoretical capacities corresponding to the formation of different Na_2S_x species. (b) The charge and discharge profiles and (c) the rate capability plot obtained at the currents of 0.2 mA, 0.5 mA, 1.0 mA, and 2.0 mA. (d) The discharge and charge voltage profiles and (e) the cycleability plot during the long-term cycling test performed at 0.5 mA.